



Deposited via The University of Sheffield.

White Rose Research Online URL for this paper:

<https://eprints.whiterose.ac.uk/id/eprint/120515/>

Version: Accepted Version

Article:

Brown, N.D., Rhodes, E.J. and Harrison, T.M. (2017) Using thermoluminescence signals from feldspars for low-temperature thermochronology. *Quaternary Geochronology*, 42. pp. 31-41. ISSN: 1871-1014

<https://doi.org/10.1016/j.quageo.2017.07.006>

Article available under the terms of the CC-BY-NC-ND licence
(<https://creativecommons.org/licenses/by-nc-nd/4.0/>).

Reuse

This article is distributed under the terms of the Creative Commons Attribution-NonCommercial-NoDerivs (CC BY-NC-ND) licence. This licence only allows you to download this work and share it with others as long as you credit the authors, but you can't change the article in any way or use it commercially. More information and the full terms of the licence here: <https://creativecommons.org/licenses/>

Takedown

If you consider content in White Rose Research Online to be in breach of UK law, please notify us by emailing eprints@whiterose.ac.uk including the URL of the record and the reason for the withdrawal request.

Using thermoluminescence signals from feldspars for low-temperature thermochronology

N.D. Brown^{a,*}, E.J. Rhodes^{a,b}, T. Mark Harrison^a

^a*Department of Earth, Planetary, and Space Sciences, University of California, Los Angeles, 595 Charles Young Drive East, Box 951567, Los Angeles, CA 90095-1567, USA*

^b*Department of Geography, Winter Street, University of Sheffield, Sheffield, South Yorkshire S10 2TN, UK*

Abstract

Natural thermoluminescence (TL) signals from feldspar crystals extracted from thermally stable drill cores ($T = -4.1 - 60.2$ °C) exhibit a strong dependence on geologic and laboratory thermal conditions. As burial temperature increases, the position of the TL glow curve at half-maximum intensity (i.e., the $T_{1/2}$ parameter) shifts to higher measurement temperatures. This shift is also observed following isothermal treatments in the laboratory. This relationship can be explained using a kinetic model originally developed for optical luminescence dating of feldspar grains. The thermal history of a sample is preserved in the degree of electron trap saturation as a function of thermal detrapping probability, which varies with recombination distance. A natural feldspar sample contains a range of thermal stabilities: the least stable traps will remain empty, the most stable will be full, and those traps which are partially filled will, in the case of thermal equilibrium, be diagnostic of the storage temperature. The $T_{1/2}$ parameter of a TL glow curve reflects which sites remain occupied. This interpretation is further borne out by additive dose measurements which illustrate that samples buried at lower temperatures are fully saturated at lower TL measurement temperatures ($\sim 200 - 300$ °C) relative to warmer samples. This signal is estimated to be useful in rapidly-cooling bedrock and should grow measurably for $\sim 10^2 - 10^6$ years.

Keywords: luminescence thermochronology, low-temperature thermochronology, feldspar thermoluminescence

1. Introduction

Luminescence signals from quartz and feldspar crystals extracted from bedrock samples have recently been shown to contain information useful for reconstructing geothermal histories (Herman

*Corresponding author

Email addresses: nathan.david.brown@ucla.edu (N.D. Brown), ed.rhodes@sheffield.ac.uk (E.J. Rhodes), tmark.harrison@gmail.com (T. Mark Harrison)

4 et al., 2010; Li and Li, 2012; Sarkar et al., 2013; Guralnik et al., 2013, 2015a,b; King et al., 2016b,c).
5 The proposed effective closure temperatures for these signals extend below 100 °C, depending on
6 the cooling rate and ambient temperature. Both quartz and feldspar luminescence signals face
7 limitations, however, in their utility as thermochronometers. The fast component of optically stim-
8 ulated luminescence (OSL) from bedrock quartz is characteristically dim, typically experiences dose
9 saturation at lower doses than feldspar, and is commonly overprinted by brighter luminescence
10 responses from inclusions, such as feldspar or zircon (Guralnik et al., 2015a). Whereas feldspar lu-
11 minescence signals are brighter and saturate at higher doses than quartz, the non-first-order kinetics
12 of detrapping (e.g., band-tail transitions, athermal fading via quantum mechanical tunneling) pose
13 a significant challenge (Jain and Ankjaergaard, 2011; Jain et al., 2015). Luminescence signals of
14 feldspar crystals extracted from crushed bedrock are the focus of this study.

15 As of yet, the only feldspar luminescence signals interrogated for thermochronometry have been
16 the infrared stimulated luminescence (IRSL) signal from Na-feldspar, extracted from the thermally-
17 stable KTB borehole in Germany (Guralnik et al., 2015b); the IRSL signal from surficial bedrock
18 feldspars collected from a range of lithologies and exhumation rates (Valla et al., 2016); and IRSL
19 signals at multiple elevated temperatures (MET) from Na- and K-rich feldspars within the rapidly-
20 exhuming eastern Himalayan syntaxis (King et al., 2016b,c). Optically-stimulated luminescence
21 techniques (including IRSL) offer several advantages for the luminescence dating of sediments in
22 comparison to thermoluminescence (TL) signals: the measured signal bleaches more rapidly with
23 sunlight exposure, and single grains can be individually stimulated with focused laser beams. How-
24 ever, for monitoring the dose response in a lightless but thermally-varying system, the TL signal
25 may provide a distinct advantage. Specifically, the stimulating energy gradually increases during
26 the measurement procedure, which produces luminescence from a continuum of thermal stabilities
27 in a single glow curve (Strickertsson, 1985; Balescu et al., 1997). Unlike IRSL techniques, which
28 stimulate with a constant optical power, TL is measured by gradually heating a sample from room
29 temperature until the relevant traps are emptied (conventionally to a maximum of around 500 °C),
30 and the luminescence emissions are monitored as a function of the temperature of the sample. Ther-
31 moluminescence emissions therefore reflect the range of occupied trap stabilities that have naturally
32 accumulated. This study aims to characterize feldspar TL as a record of geothermal history.

33 Thermoluminescence has long been used to discern features about a sample’s thermal history.
34 Most often, researchers are interested in the time since the thermal-resetting of archaeological
35 materials. Quartz is the more common target mineral in this context. Target materials include

36 fired ceramics (Aitken et al., 1964; Fleming et al., 1970), hearth stones (Plachy and Sutton, 1982),
37 and burnt flint (Valladas and Valladas, 1987). A notable exception is the use of feldspar TL for the
38 dating of burnt stones and ceramics (Mejdahl, 1983, 1985; Spencer and Sanderson, 1994, 2012).

39 When used for thermochronometry, thermoluminescence studies usually consider the decay of
40 peaks in quartz crystals (e.g., Tang and Li, 2015). Prokein and Wagner (1994) observed the reduc-
41 tion of the quartz 325 °C TL peak over a wide range of steady-state temperatures (14 - 56 °C), and
42 Nambu et al. (1996) made the more general observation of decreasing overall quartz TL intensity
43 with burial temperature, an observation that was given more robust theoretical treatment in later
44 work (Tsuchiya et al., 2000; Tsuchiya and Fujino, 2000; Schmidt et al., 2015). Gong et al. (2010)
45 extended the ESR framework of Grün et al. (1999) to estimate apparent ages and paleotemperatures
46 for the 375 and 425 °C TL peaks of quartz from sedimentary basins. Ypma and Hochman (1991)
47 monitored the temperature shift of the bulk TL glow curve in quartz from sedimentary basins and
48 noticed systematic shifts between basins with differential exhumation histories.

49 Thermoluminescence signals from lunar rocks and fines (e.g., plagioclase) have also been used
50 to estimate the balance between irradiation and thermal depletion of traps. These studies produced
51 quantitative estimates of sediment burial depth (Hoyt et al., 1970; Durrani et al., 1973), effective
52 storage temperature (Durrani et al., 1972, 1973), thermal gradient (Hoyt et al., 1971), and even
53 the duration of shadow cover for samples adjacent to boulders (Durrani et al., 1977). The present
54 study extends that body of work by incorporating recent advances in the understanding of feldspar
55 luminescence kinetics (e.g., detrapping by tunneling to nearby recombination centers; Jain et al.,
56 2015) and by considering long-term storage of feldspars at upper-crustal temperatures in terrestrial
57 drill cores.

58 This study examines both the natural and laboratory-induced TL signals from feldspar crystals
59 extracted from split drill cores originally collected from Alaska, Colorado, and Wyoming that rep-
60 resent steady-state heat flows of 54.4, 58.3, and 100.4 mW/m², respectively. First, the TL signals
61 of feldspars taken from different depths are measured. The natural signals are presented along
62 with multiple-aliquot additive-dose (MAAD) and single-aliquot regenerative (SAR) dose responses,
63 as well as isothermal decay measurements. Next, these signals are compared with results from a
64 kinetic model similar to that of Jain et al. (2015) that assumes that: a) distance-dependent, excited-
65 state tunneling is the primary pathway for feldspar luminescence; and b) that sites at increasing
66 distances from centers will exhibit greater trapping stability. We simulate laboratory and natural
67 isothermal conditions and compare the simulated results to our measurements. Finally, we suggest

68 future research directions.

69 **2. Materials and methods**

70 *2.1. Geologic context and sample collection*

71 A total of 20 samples were collected from split drill cores kept at the United States Geologic
72 Survey Core Research Center (CRC), Lakewood, Colorado. The samples were chosen to repre-
73 sent a wide range of steady-state temperatures ($-4.1 - 60.2$ °C), within relatively uniform litholo-
74 gies. The three cores sampled were from the North Slope of Alaska (CRC library code E802;
75 $n = 5$; $69^{\circ}50'18''\text{N}$, $155^{\circ}59'24''\text{W}$), the Piceance Basin of northwestern Colorado (W219; $n = 8$;
76 $39^{\circ}53'36''\text{N}$, $108^{\circ}32'37''\text{W}$), and the Greater Green River Basin of south-central Wyoming (R716;
77 $n = 7$; $41^{\circ}2'41''\text{N}$, $108^{\circ}6'39''\text{W}$) (Fig. 1(a) and (b)).

78 Core E802 from the Colville Basin of North Slope Alaska is comprised of the Nanushuk Group:
79 Lower and Upper Cretaceous sandstone, shale, and minor conglomerate deltaic wedge, all shed from
80 the Brooks Range, a series of thrust sheets stacked during the Late Jurassic to Early Cretaceous
81 arc-continent collision (Mull et al., 1987). Core W219 is comprised of the Green River Forma-
82 tion: Eocene interbedded mudstone and sandstone, carbonaceous shale, lenticular sandstones and
83 thickly-bedded evaporites that were deposited in and around lacustrine basins formed during the
84 Laramide orogeny (Irwin, 1977; Smith et al., 2008). Core R716 contains Eocene basin-fill (Wasatch
85 Formation): floodplain deposits of lenticular of parallel-bedded sandstones, and mudstone (Roehler,
86 1992). Similar to W219, the R716 core was likely derived from Laramide basement (Fan et al., 2011).

87 To estimate the undisturbed modern subsurface temperatures for each core, the following steps
88 were taken. For E802, the geothermal gradients above and below the ice-bearing permafrost layer
89 were interpolated from nearby sites within the Colville Basin which were measured for a high-
90 resolution temperature survey of wells considered to be in thermal equilibrium (Collett et al., 1993).
91 For W219, a similar interpolation was performed using gradient-at-depth measurements from nearby
92 sites within the Piceance Basin (Blackwell et al., 2011). For R716, a geothermal gradient map was
93 used (Finn, 2005). From these geothermal gradient approximations, the modern temperature of
94 each core sample was estimated (Fig. 1(b)). Further details about these measurements can be
95 found in the Supplementary Materials.

96 Whether samples are in thermal equilibrium depends on the exhumation rate at each core site.
97 The most rapid exhumation is at site W219. Although no measurements have been made at the
98 core site itself, fluid inclusion microthermometry (Fall et al., 2012, 2015) and vitrine reflectance

99 data (Zhang et al., 2008) from the center of the Piceance Basin imply an exhumation rate of 0.16
100 - 0.24 km/Ma since 10 Ma, corresponding to a cooling rate of 3.8 °C/Ma within the Mesaverde
101 Group (modern geothermal gradient of 53 °C/km), immediately below the Wasatch Formation
102 (vitrine reflectance data suggest heat-flow values similar to modern since the Miocene). Moreover,
103 the exhumation at the northern basin edge is expected to be slower than in the center (Zhang
104 et al., 2008). Based on apatite fission track cooling ages, the exhumation rate for the Colville Basin
105 (core E802) since the Paleocene has been about 0.05 - 0.06 km/Ma (Cole et al., 1997) and vitrine
106 reflectance data suggest an exhumation rate of 0.01 - 0.02 km/Ma since the Eocene for the Green
107 River Basin (core R716) (Jagniecki et al., 2013), both of which are effectively static for the TL signal
108 considered here. The modern geothermal gradients at these sites are also much lower than at W219:
109 34 and 35 °C/km compared with 53 °C/km (see Supplementary Materials for more detail), which
110 would result in cooling rates of 1.9 and 0.5 °C/Ma for E802 and R716, respectively. Because these
111 cooling rates are considerably lower than the reported detectable cooling rates for other trapped-
112 charge thermochronometric systems (e.g., >20 to 615 °C/Ma; Table 2 of King et al., 2016a), the
113 modern undisturbed core temperature measurements are reported as ‘steady-state’ temperatures
114 (T_{SS}) hereafter.

115 2.2. Sample preparation and instrumentation

116 To isolate the inner portion of the split drill cores, the samples were spray-painted and then the
117 outer surfaces were removed using a rotary tool fitted with a tile-cutting bit. The unexposed inner
118 portions from the drill core samples were then ground with a pestle and mortar and sieved to isolate
119 the 175 - 400 μm size fraction. These separates were then treated with 3% hydrochloric acid and
120 separated by density using lithium metatungstate heavy liquid ($\rho < 2.565 \text{ g/cm}^3$; Rhodes 2015) in
121 order to isolate the most potassic feldspar crystals. Crystals were mounted on stainless steel discs
122 in a small-diameter (3 - 5 mm) monolayer using silicon oil.

123 The outer portions of each sample were analyzed with inductively-coupled plasma mass spec-
124 trometry (ICP-MS) to estimate the U and Th contents, and with inductively-coupled optical emis-
125 sion spectrometry (ICP-OES) to measure the K content. These values were converted into a geologic
126 dose-rate using the factors of Adamiec and Aiken (1998). We estimate an internal dose-rate assum-
127 ing a feldspar potassium content of $12.5 \pm 0.5 \text{ wt}\%$ (Huntley and Baril, 1997). Beta attenuation
128 is calculated assuming a water content of $0.5 \pm 0.5\%$. The resulting geologic dose-rate values are
129 listed in Table 1.

Table 1: Sample depths, steady-state temperatures, and dose-rate information.

Field code	Lab code	Depth (m)	T_{SS} ($^{\circ}\text{C}$)	K (%)	Th (ppm)	U (ppm)	Total dose-rate (Gy/ka)
E802-1	J1012	159	-4.1	1.1	5.2	2.04	2.85 ± 0.11
E802-2	J1013	303	0.8	0.9	3.5	1.39	2.39 ± 0.10
E802-3	J1014	367	3.0	1.1	4.9	1.77	2.76 ± 0.11
E802-4	J1015	496	7.4	1.3	5.5	1.96	3.04 ± 0.12
E802-5	J1016	656	12.8	0.9	6.1	2.09	2.73 ± 0.10
W219-1	J1017	7	6.4	3.6	9.7	2.39	5.72 ± 0.27
W219-2	J1018	72	9.8	2.4	10.0	1.87	4.36 ± 0.19
W219-3	J1019	150	14.0	6.1	7.2	2.13	7.71 ± 0.43
W219-4	J1020	240	18.7	1.3	4.6	4.21	3.49 ± 0.13
W219-5	J1021*	321	23.0	1.6	3.5	2.34	3.27 ± 0.14
W219-6	J1022*	418	28.2	1.3	4.8	2.47	3.11 ± 0.12
W219-7	J1023*	509	33.0	2.2	12.1	3.55	4.70 ± 0.18
W219-8	J1024*	575	36.5	0.4	1.9	0.98	1.72 ± 0.08
R716-1	J1025	307	15.1	2.1	7.1	1.57	3.81 ± 0.17
R716-2	J1026	445	19.8	2.5	17.1	4.81	5.61 ± 0.21
R716-3	J1027	606	25.4	2.4	16.4	3.59	5.19 ± 0.20
R716-4	J1028	881	35.0	2.1	23.8	5.43	5.83 ± 0.21
R716-5	J1029	1030	40.1	1.9	13.8	2.82	4.36 ± 0.17
R716-6	J1030	1462	55.1	1.9	16.9	3.68	4.77 ± 0.18
R716-7	J1031	1609	60.2	0.9	3.2	2.15	2.60 ± 0.10

*The natural signals from these samples were conflated with black-body radiation emissions during measurement and are disregarded from further analysis.

130 Luminescence measurements were carried out at the UCLA luminescence laboratory using a
131 TL-DA-20 Risø automated reader equipped with a $^{90}\text{Sr}/^{90}\text{Y}$ beta source. Thermoluminescence
132 emissions were detected through a Schott BG3-BG39 filter combination (transmission window of
133 325 - 475 nm) in a nitrogen atmosphere.

134 3. Thermoluminescence signals from feldspars extracted from drill cores

135 3.1. Natural signals

136 Sixteen of the 20 measured samples produced natural TL signals suitable for analysis (Fig. 2).
137 The four rejected samples were from core W219, were buried at temperatures ≥ 23 °C, and yielded
138 natural signals dominated by black-body radiation (approximated by measuring TL from the same
139 aliquot after the natural signal has been removed). This lack of natural signal likely results from the
140 high burial temperatures experienced by these samples. In core R716, however, samples with higher
141 T_{SS} values retained natural TL signals above black-body radiation levels. The natural variability
142 in the upper limit of resolvable T_{SS} values deserves further exploration.

143 Because the low-temperature TL peak in feldspar is generally asymmetric with overlapping
144 peaks at higher temperatures, it is common practice to describe natural TL curves according to the
145 measurement temperature at half of the maximum TL intensity (i.e., the position of the ‘leading
146 edge’ of the main peak in a TL glow curve), or $T_{1/2}$ (e.g., Spencer and Sanderson, 2012). As steady-
147 state temperatures (T_{SS}) increase, the natural $T_{1/2}$ values shift to higher temperatures (Fig. 1c).
148 Additionally, within a given core (each of which has a fairly uniform lithology), TL brightness tends
149 to decrease at higher T_{SS} values (Fig. 2).

150 3.2. Field saturation

151 A primary concern when considering the dose-response characteristics of luminescence signals is
152 a change in sensitivity during the course of a measurement sequence (Wintle and Huntley, 1982).
153 To avoid any such changes in the dose-response sensitivity induced by heating, we tested the level
154 of natural dose-saturation (i.e., ‘field saturation’; Kars et al., 2008) in samples J1012 and J1030 by
155 using a multiple-aliquot additive-dose (MAAD) approach. Separate aliquots were given beta doses
156 in addition to their natural doses. The subsequent TL curves (Fig. 3a - b) show which regions of
157 the glow curve are saturated (and do not, therefore, grow with dose) and which regions are not
158 saturated (and grow with dose).

159 Sample J1012 is almost fully saturated from about 270 to 370 °C, with an average ratio of $0.95 \pm$
160 0.02 . Sample J1030 shows a similar degree of saturation, 0.95 ± 0.03 , from 340 to 410 °C (Fig. 3c).
161 The key observation from this experiment is that T_{SS} relates to the TL measurement temperature
162 at which traps are fully saturated (i.e., in field saturation; $T_{SS} = -4.1$ °C for J1012 and 55.1 °C for
163 J1030). This indicates that burial temperature controls which regions within a TL curve are stable
164 enough to accumulate charge over time. At higher measurement temperatures, both samples show

165 ratios greater than one, which may reflect the effect of dose-quenching (for a detailed description of
 166 this phenomenon in quartz, see Bailey, 2001) on a high-temperature peak (e.g., 410 °C TL peak;
 167 Murray et al., 2009). Why the samples are > 1 at different temperatures is unclear, but likely
 168 relates to the variability in the position of the high-temperature peak(s).

169 3.3. Signals following isothermal treatments

170 After the measurement of the natural signal, an aliquot of sample J1012 (core E802) was given
 171 a beta dose of 24 Gy and then subjected to a series of isothermal treatments: 50, 100, 150, and
 172 200 °C for 10, 30, 100, 300, and 1000 s. Following these treatments, the TL signals were measured
 173 (Fig. 4). A shift to higher temperatures for the $T_{1/2}$ value and a reduction in TL intensity result
 174 from longer heat treatments and greater hold temperatures, an observation made previously (e.g.,
 175 Spencer and Sanderson, 1994). This resembles the effect of burial at higher natural T_{SS} values
 176 (Fig. 2). Both of these effects are simulated later in this work in sections 4.3 and 4.4.

177 A higher temperature peak is evident, centered around 390 °C. High-temperature peaks (cen-
 178 tered between $\sim 310 - 410$ °C) are well-documented for feldspar TL studies and exhibit different
 179 luminescence properties than the lower-temperature peak and probably therefore involve a differ-
 180 ent combination of traps and/or recombination centers (Balescu et al., 1991; Duller, 1994, 1997;
 181 Murray et al., 2009). For that reason, our analysis is restricted to those regions unaffected by this
 182 higher-temperature peak.

183 4. A kinematic model of feldspar TL

184 4.1. Model description

In this study, we estimate the net change in the concentration of trapped electrons with the following expression

$$\frac{dn(r')}{dt} = \frac{\dot{D}}{D_0} \left(N(r') - n(r') \right) - n(r') \exp \left(- \Delta E / k_B T \right) \frac{P(r')s}{P(r') + s} \quad (1)$$

The accumulation term for every dimensionless recombination distance r' depends on the concentration of unoccupied traps ($N(r') - n(r')$), which will fill at a rate proportional to the dose-rate \dot{D} (Gy/s), normalized by D_0 , the dose (Gy) at which $(1 - e^{-1})$ of the total traps are filled (i.e., the characteristic dose) (Christodoulides et al., 1971). The total concentration of traps separated from a recombination center by some distance between r' and $r' + dr'$ is given by Huntley (2006) as

$$N(r')dr' = N \cdot 3(r')^2 \exp \left(- (r')^3 \right) dr' \quad (2)$$

Table 2: Parameter values used in kinetic model.

Parameter	Description	Value
\dot{D}	Dose rate	4 Gy·ka ⁻¹ (geologic) or 0.1 Gy·s ⁻¹ (laboratory)
D_0	Characteristic dose	1.6 kGy
ΔE	Activation energy to excited state	1.3 eV
P_0, s	Frequency factors	$2 \times 10^{16} \text{ s}^{-1}$
ρ'	Dimensionless recombination center density	1.32×10^{-3}

The loss term multiplies the concentration of trapped electrons at some distance $n(r')$ by their recombination probability. Following recent work (Jain et al., 2015; Pagonis et al., 2016), we approximate the detrapping probability in feldspar as localized transitions to randomly-distributed luminescence centers. This probability is governed by the activation energy from the ground- to the excited-state, ΔE (eV), the temperature of the lattice, T (K), the attempt-to-escape frequency factor, s (s⁻¹), and the excited-state tunneling probability, $P(r')$ (s⁻¹). The tunneling probability decreases with r' according to the relationship

$$P(r') = P_0 \exp(-\rho'^{-1/3} r') \quad (3)$$

185 where P_0 (s⁻¹) is the attempt-to-tunnel probability and ρ' the dimensionless concentration of re-
 186 combination centers in the lattice (Huntley, 2006). A more complete model description is found in
 187 the Supplementary Materials.

By numerically solving Equation 1 for geothermal or laboratory conditions, we can evaluate how the trapped electron population, $n(r')$, evolves through time (all simulations presented in this work were evaluated with the ode23tb solver within MATLAB). The resulting $n(r')$ array can then be taken as the input for a simulated TL measurement. The expression for TL intensity as a function of measurement time is given as

$$I_{TL}(t) \propto \int_{t=0}^{t_F} \int_{r'=0}^{\infty} n(r') dr' dt \quad (4)$$

188 when a sample is heated from $T = 0$ to T_F at $dT/dt = \beta$ °C/s. The final measurement time, t_F , is
 189 the final temperature, T_F , divided by the heating rate, β .

190 4.2. Model parameter values

191 The behavior of Eq. 1 is sensitive to the parameter values chosen. In this section, we describe
 192 the values used in this study. While all of the values presented here are consistent with available

193 literature values and with experimental results, it should be stressed that many of these values will
194 vary between samples. The careful quantification of these parameters will be a prerequisite for the
195 quantification of thermal histories using feldspar TL signals.

196 4.2.1. Geologic (\dot{D}_G) and laboratory (\dot{D}_L) dose rates

197 The average environmental dose rate for all samples is 4.0 ± 1.5 Gy/ka, represented by our
198 chosen \dot{D}_G value of 4 Gy/ka. The laboratory dose rate, \dot{D}_L , administered by the $^{90}\text{Sr}/^{90}\text{Y}$ beta
199 source at UCLA has been measured to be 0.1 Gy/s at the sample location using the standard
200 calibration quartz sample supplied from Risø DTU National Laboratory. This value is used to
201 simulate laboratory irradiations.

202 4.2.2. Characteristic dose, D_0

The TL dose response of sample J1012 is shown in Fig 5(a) following single-aliquot regenerative
doses ranging from 0 to 3.9 kGy. Because we are concerned with growth in the region of the TL
curve near the natural $T_{1/2}$ values, we examine the saturation behavior around the 230 °C region
of the glow curves ($T_{1/2} = 223, 223, 227,$ and 236 °C for J1012; purple TL curves in Fig. 2).
Specifically, we fit the TL values to a single saturating exponential function of the form

$$I = I_{max}(1 - \exp^{-D/D_0}) \quad (5)$$

203 where I is the TL intensity which increases with given dose D up to some maximum intensity I_{max}
204 (Christodoulides et al., 1971). In this region, we see an average D_0 value of 1.6 kGy. Such a value
205 is consistent with previous additive dose observations (e.g., Balescu and Lamothe, 1992; Balescu
206 et al., 1997).

207 Given the multiple-aliquot additive-dose (MAAD) results reported in the Section 3.2, it appears
208 as though the TL intensity at the natural $T_{1/2}$ value derives from those traps which will remain only
209 partially filled ($n/N < 0.86$) at the relevant geologic dose-rate and temperature. In this view, a
210 conservative approach would be to examine the dose-responses at more stable portions of the curve
211 to avoid measuring traps that would fill at laboratory but not geologic dose-rates. We therefore
212 report a D_0 value of 1.6 kGy, a value taken from the range $260 < T$ (°C) < 270 .

213 Ultimately, this parameter will control the time required for a sample to equilibrate to thermal
214 steady-state and should therefore be quantified thoroughly when addressing transient responses to
215 thermal perturbation. For our study, where sites have been cooling very slowly for at least 10
216 Ma ($t \gg 2D_0/\dot{D}$), this parameter will not significantly affect our drill core fitting results. In

217 rapidly-cooling bedrock, however, this term will influence the length of time that traps will remain
 218 in disequilibrium.

219 4.2.3. Frequency factors, P_0 and s

220 For the attempt-to-tunnel and attempt-to-escape frequency factors (P_0 and s , respectively) we
 221 use a reasonable but arbitrary value of $2 \times 10^{16} \text{ s}^{-1}$. Post-isothermal TL analyses (Brown and
 222 Rhodes, 2017) of J1012 suggest that the effective frequency factors involved in TL production, i.e.,
 223 $(P(r')s)/(P(r')+s)$ term within Equation 1, range from 10^{14} to 10^{18} s^{-1} , decreasing monotonically
 224 as a function of isothermal holding temperature or duration.

225 Despite the fact that the P_0 and s values have different physical meanings (pp. 48-49, McKeever,
 226 1985; Tsuchiya et al., 1987) and may vary by orders of magnitude (Jain et al., 2015), we assign them
 227 the same numerical value for goodness-of-fit and simplicity (we express both terms individually in
 228 Equation 1).

229 4.2.4. Activation energy, ΔE , and recombination center density, ρ'

Jain et al. (2015) introduced the following expression to describe isothermal TL from feldspars:

$$L \propto -\frac{dn}{dt} = 3n_0\rho'z(t')^{-1} \left(\ln(t'P_0) - \xi \right)^2 \exp \left(-\rho' \left(\ln(t'P_0) - \xi \right)^3 \right) \quad (6)$$

230 where $t' = \tau_0 + zt$ and $\xi = \Delta E/k_B T$, with n_0 representing the concentration of trapped electrons at
 231 the start of the measurement and z representing the rate of change for the lifetime of trapped charge
 232 (following Huntley (2006) and Jain et al. (2012), we set $z = 1.8$). The variable τ_0 represents the
 233 critical lifetime at the start of the measurement. Both n_0 and τ_0 depend upon the radiation history of
 234 a sample and are best-fit parameters. Assuming that recombination proceeds by tunneling from the
 235 excited state to randomly-distributed luminescence centers, isothermal TL at any hold temperature
 236 should approximately follow Eq. 6.

237 Fig. 5(b) shows the isothermal decay of an aliquot of J1012 held at 250, 300, and 350 °C for
 238 1000 s (400 s of which is shown). These data are fitted with Eq. 6 using the same parameters used
 239 in the main text to fit the $T_{1/2}$ values for all drill core samples at natural and laboratory conditions,
 240 namely: $\Delta E = 1.3 \text{ eV}$, $\rho' = 1.32 \times 10^{-3}$ and $P_0 = 2 \times 10^{16} \text{ s}^{-1}$.

241 4.3. Simulated TL responses following isothermal geologic histories

242 Using Eq. 1 and the parameter values listed in Table 2 (with the average geologic dose rate
 243 \dot{D}_G for all samples of 4 Gy/ka), we modelled the evolution of $n(r')$ for hold temperatures of 0,

244 10, and 20 °C, and durations of 20 ka, 200 ka, and 2 Ma. After 800 ka ($2D_0/\dot{D}_G$), assuming the
245 parameters listed in Table 2, the most stable traps (highest r' values) will be effectively saturated,
246 i.e., $n/N \sim 0.86$ (see also Fig. 7). After 2 Ma, these traps should be entirely full ($n/N \sim 1$). The
247 final distribution of $n(r')$ after each treatment was then evaluated using Eq. 4 to produce a synthetic
248 TL curve; these are shown in Fig. 6a.

249 Two features are remarkable. First, and most relevant for this study, the TL peaks are emitted
250 at higher stimulation temperatures when trapping occurs at higher temperatures. This is because
251 those sites which are nearer to centers (i.e., have lower r' values) are unstable at higher ambient
252 temperatures, and are therefore empty during the natural TL measurement. Second, the integrated
253 emissions are greater for those simulations at lower temperatures. The reason for this is that the
254 ratio of excited-to-ground-state electrons (n_e/n_g) depends exponentially on temperature ($n_e/n_g =$
255 $\exp(-\Delta E/k_B T)$) and this ratio controls the rate of detrapping (see the Supplementary Materials
256 for more detail).

257 *4.4. Simulated TL responses following isothermal treatments*

258 The same approach was used to predict the effects of short duration heat treatments. For each
259 of these simulations, laboratory irradiation was reproduced by changing the dose rate, \dot{D} , to 0.1
260 Gy/s (this mimics the dose-rate received by crystals exposed to the $^{90}\text{Sr}/^{90}\text{Y}$ beta source at UCLA)
261 and allowing the $n(r')$ distribution to evolve for 200 s (a simulated laboratory dose of 20 Gy) at 20
262 °C. Next, this $n(r')$ distribution was used as the initial condition of an isothermal heat treatment.
263 The simulated hold times were 100, 300, and 1000 s; and the temperatures were 100, 150, and 200
264 °C. Finally, the $n(r')$ distribution was evaluated with Eq. 4, producing the TL curves shown in
265 Fig. 6c.

266 The effects of heating are to shift the TL emissions to higher measurement temperatures and
267 to reduce the peak intensity. This reason for this behavior is the progressive thermal erosion of
268 those sites which have lower recombination distances; the more stable sites comprise the higher
269 temperature regions of the TL measurements.

270 *4.5. Trapping at a single recombination distance*

271 Equation (1) can also be used to illustrate the evolution of trap populations under different
272 scenarios. An arbitrary recombination distance of r' (e.g., 1.5) and a constant temperature of
273 -4.1 °C (e.g., sample J1012) are examined within a 2 Ma simulation (Fig. 7a). The results are
274 shown as the fraction of traps which are filled (when $n/N = 1$, all available traps are filled). Once

275 about 86% of traps are filled, even small variations in the measured luminescence response will
276 lead to large or infinite errors in age determination and the trap is effectively saturated (Wintle
277 and Murray, 2006). This saturation level is described with the D_0 parameter (effective saturation
278 occurring at doses $> 2D_0$). In our case, we prescribe a value of $D_0 = 1.6$ kGy based on dose
279 response measurements of sample J1012 (Fig. 5a); higher values result in a greater time required to
280 reach saturation.

281 In our simulation, trap filling through time progresses as expected for a discrete trap (Fig. 7a). As
282 the available sites fill, the fractional saturation behaves as a saturating exponential function. Notice
283 that at the chosen temperature, this site will not fill entirely ($n/N < 1$). In other words, a thermal
284 steady-state ($(n/N)_{SS}$) is reached which is incompletely saturated (cf. Christodoulides et al., 1971).
285 Of course, with randomly distributed luminescence centers many recombination distances will occur,
286 as discussed in the following section.

287 *4.6. Trapping at all recombination distances*

288 Considering all recombination distances present in the lattice and assuming randomly distributed
289 centers, we can visualize trapping as a function of both time and recombination distance. Using
290 Eq. 1, trapping is simulated at $T = -4.1^\circ\text{C}$ for durations of 0.25, 0.5, 1, and 2 Ma (Fig. 7b).
291 The results shown in Fig. 7a are indicated with the light blue line for reference. Those traps with
292 centers nearer than about $r' = 1.7$ will not saturate completely (given the prescribed temperature
293 and dose rate) and sites at $r' \lesssim 0.8$ will not accumulate a significant concentration of electrons. Such
294 sites would accumulate appreciable charge, however, if the temperature were lowered sufficiently.
295 Nevertheless, after 2 Ma all sites are in thermal steady-state ($(n/N)_{SS}$) and their concentrations
296 will not change until the temperature changes.

297 *4.7. Trapping at drill core temperatures*

298 Finally, the simulation conducted in Section 4.6 is repeated for the steady-state temperatures
299 experienced by drill core samples J1012, J1026, and J1030 ($T_{SS} = -4.1, 19.8,$ and 55.1°C , respec-
300 tively) (Fig. 7c). The r' values greater than about 1.48 reach effective saturation ($n/N > 0.86$) after
301 some amount of time (in this example, sites nearer to centers than $r' = 1.48$ experience thermally-
302 assisted tunneling at a rate higher than the filling rate). The more stable sites saturate after 800
303 ka, but some of the less stable sites reach saturation later. This is because the detrapping rate is
304 greater for these sites.

305 Higher mean temperatures result in a trapped population with greater minimum r' values. In
306 other words, the nearer sites that would be occupied at lower temperatures remain empty at higher
307 temperatures. This trend in site occupancy with temperature can be examined in the measured TL
308 signals from drill core samples, which is discussed in the following section.

309 5. Comparing measured and modeled behaviors

310 5.1. Comparing natural signals to modeled signals

311 The $T_{1/2}$ values for all drill core natural TL signals are shown as open symbols in Fig. 6b.
312 Also shown as a solid black curve in Fig. 6b are the $T_{1/2}$ values simulated at natural conditions.
313 To produce these values, we first solve Eq. 1 for the time range $t = 0$ to 2 Ma at each sample's
314 burial temperature, T_{SS} . The resulting $n(r')$ distribution for each sample is evaluated with Eq. 4
315 to determine the TL that would result after burial at T_{SS} for 2 Ma. A remarkable correlation is
316 found, suggesting that the measured relationship between natural $T_{1/2}$ values and the steady-state
317 temperature is explainable in terms of site stability.

318 5.2. Comparing isothermal decay of TL signals to modeled response

319 The $T_{1/2}$ values following laboratory irradiation and heat treatment are plotted as open symbols
320 in Fig. 6d. Also plotted are the $T_{1/2}$ values that are simulated with Eqs. 1 and 4, given the
321 same kinetic parameters used in Fig. 6b. It is encouraging that the same kinetic parameters that
322 reproduce the natural drill core $T_{1/2}$ values also resemble the high-temperature measurements.

323 This correlation between measured and simulated $T_{1/2}$ values gets stronger at longer durations
324 and higher temperatures, which may suggest that our model fails to incorporate transient lumi-
325 nescence phenomena occurring at room temperature. Ground-state tunneling is omitted from the
326 current model, but this effect should only decrease the minimum stability distance, shifting the $T_{1/2}$
327 value higher. This discrepancy deserves further consideration.

328 6. Discussion and Conclusions

329 Thermoluminescence signals from bedrock feldspars show a systematic dependence on ambient
330 temperature. During burial, the electron traps within these crystals were filled according to the
331 stability of each trapping site. Because this stability should depend on the distance to the nearest
332 recombination center, a distribution of trap saturation as a function of distance develops, $n(r')$,
333 which characterizes a samples thermal history. In the case of thermal steady-state, some sites

334 are entirely filled ($n/N \sim 1$), some are partially filled, and some remain empty (Fig. 7b). This
335 partially-occupied recombination distance controls the position of the $T_{1/2}$ measurements shown for
336 the natural signals and for signals following isothermal treatments (Figs. 6b and d).

337 The systematic dependence of natural $T_{1/2}$ values on ambient temperature (Fig. 6b) coupled
338 with the multiple-additive dose results (Fig. 3) imply that T_{SS} controls trapping site occupancy
339 and therefore the natural shape of feldspar TL, a behavior that can be explained in light of recent
340 advances in our understanding of feldspar luminescence kinetics (e.g., Jain et al., 2015; Pagonis et al.,
341 2016). Within this context, the role of anomalous fading should be considered. In our formulation
342 (Eq. 1), fading is incorporated, though only in the excited-state (i.e., thermally-assisted tunneling).
343 Thermally-activated tunneling can produce the phenomenon of anomalous fading as commonly
344 measured in sediment studies (e.g., a decrease in luminescence intensity after storage at room
345 temperature; Huntley and Lamothe, 2001), though with current parameter values, the magnitude
346 of simulated room temperature fading is much lower than is experimentally observed. The observed
347 fading rate will depend primarily upon the activation energy required to access the excited state,
348 the ambient temperature, the effective frequency factor, and the density of recombination centers.

349 Of particular note is the agreement that we observe between model predictions and measured TL
350 responses following natural and high-temperature laboratory heating conditions (Fig. 6). The same
351 kinetic parameters (Table 2) described in Section 4.2 can be evaluated with Eq. 1 to reproduce the
352 $T_{1/2}$ position resulting from 1000 s at 200 °C ($T_{1/2}$ offset by 15 °C; Fig. 6d) and thermal steady-state
353 ($t \gtrsim$ order 10^5 ka) at -4.1 °C ($T_{1/2}$ offset by 5 °C; Fig. 6b).

354 We emphasize that this model is one of the simplest justifiable models for feldspar luminescence.
355 Additional pathways that could be incorporated in the future might include activation into the band-
356 tail states (up to the conduction band) or ground-state tunneling, both of which have been adopted
357 for IRSL thermochronometry with feldspars (e.g., Guralnik et al., 2015b; King et al., 2016b). The
358 main elements of this kinetic model are identical to those used in Jain et al. (2015) and have
359 been used in that and other studies (Kitis and Pagonis, 2013; Pagonis et al., 2016) to explain
360 both optical and thermal features of feldspar luminescence. Thermoluminescence signals may be
361 preferable over optical luminescence for feldspar thermochronology applications, however, as the
362 full range of thermal stability is monitored during a single TL measurement. Additionally, TL
363 measurements avoid the complications arising from preheating and phototransfer effects.

364 Moving forward, many questions remain to fully develop this method. Does the feldspar TL re-
365 sponse become more sensitive to radiation with prolonged heating or metamorphism? Both the TL

366 shape change after heating to 500 °C (Brown, 2017) and the observation that the degree of feldspar
367 ordering correlates with the degree of fading (p. 189, Aitken, 1985; Visocekas et al., 1994) suggest
368 that peak metamorphic conditions may influence the subsequent rate of charge accumulation. What
369 is the maximum steady-state temperature that can be identified using the leading edge of TL emis-
370 sions? In core W219, the natural TL signals were too low to resolve the $T_{1/2}$ value at $T \geq 23.0$ °C,
371 whereas for core R716, all samples gave useful TL signals, up to the highest temperatures measured:
372 60.2 °C. How should one handle low-temperature shoulders when identifying the natural $T_{1/2}$ value?
373 It may be useful to separate shoulders by curve deconvolution, for example. Can we analytically
374 define the closure temperature for a TL age resulting from different geothermal scenarios, or can this
375 only be defined numerically? What is the natural variation for the parameters of Table 2? Efforts
376 are underway currently to explore this variation for both optical and thermal signals in feldspars
377 (Sfampa et al., 2015; Guralnik et al., 2015b; Valla et al., 2016; Brown and Rhodes, 2017). Is excited-
378 state tunneling to randomly-distributed luminescence centers the primary detrapping pathway at
379 geologic conditions? For example, initial simulations of linear cooling scenarios (not shown here)
380 indicate that the TL system presented here may remain in thermal disequilibrium at cooling rates
381 as slow as about 10 °C/Ma, but this result depends strongly on the parameter values chosen as well
382 as the incorporated recombination pathways.

383 Our results illustrate the potential utility of the feldspar TL signal for geothermal studies. The
384 $n(r')$ distribution is sensitive to a wide range of ambient temperatures: $-4.1 - 60.2$ °C. This dis-
385 tribution responds to thermally dynamic scenarios as well and initial simulations suggest that the
386 signal should be useful for monitoring rapid exhumation during the Quaternary. This combination
387 of low-temperature sensitivity and measurable signal growth between 10^2 to 10^6 years is promising
388 for tectonic and geomorphic applications involving short-wavelength, upper-crustal thermal pertur-
389 bations, and could prove useful in resolving questions of recent bedrock exhumation rates.

390 **Acknowledgements**

391 We thank Pierre Valla and Benny Guralnik for their insightful comments which have signifi-
392 cantly improved this work. We also thank the USGS Core Research Center for providing drill core
393 subsamples for analysis.

394 **References**

395 Adamiec, G., Aitken, M., 1998. Dose-rate conversion factors: update. *Ancient TL* 16, 37–50.

- 396 Aitken, M., 1985. Thermoluminescence Dating. Academic Press, London.
- 397 Aitken, M., Tite, M., Reid, J., 1964. Thermoluminescent dating of ancient ceramics. *Nature* 202,
398 1032–1033.
- 399 Bailey, R., 2001. Towards a general kinetic model for optically and thermally stimulated lumines-
400 cence of quartz. *Radiation Measurements* 33, 17–45.
- 401 Balescu, S., Lamothe, M., 1992. The blue emission of K-feldspar coarse grains and its potential for
402 overcoming TL age underestimation. *Quaternary Science Reviews* 11, 45–51.
- 403 Balescu, S., Lamothe, M., Lautridou, J.P., 1997. Luminescence evidence for two Middle Pleistocene
404 interglacial events at Tourville, northwestern France. *Boreas* 26, 61–72.
- 405 Balescu, S., Packman, S.C., Wintle, A.G., 1991. Chronological separation of interglacial raised
406 beaches from northwestern Europe using thermoluminescence. *Quaternary Research* 35, 95–102.
- 407 Blackwell, D., Richards, M., Frone, Z., Batir, J., Ruzo, A., Dingwall, R., Williams, M., 2011. Tem-
408 perature at depth maps for the conterminous US and geothermal resource estimates. *Geothermal*
409 *Resources Council Transactions* 35, 1545–1550.
- 410 Brown, N.D., 2017. Using luminescence signals from bedrock feldspars for low-temperature ther-
411 mochronology. Ph.D. thesis. University of California, Los Angeles.
- 412 Brown, N.D., Rhodes, E.J., 2017. Thermoluminescence measurements of trap depth in alkali feldspars
413 extracted from bedrock samples. *Radiation Measurements* 96, 53–61.
- 414 Christodoulides, C., Ettinger, K.V., Fremlin, J.H., 1971. The use of TL glow peaks at equilibrium
415 in the examination of the thermal and radiation history of minerals. *Modern Geology* 2, 275–280.
- 416 Cole, F., Bird, K.J., Toro, J., Roure, F., O’Sullivan, P.B., Pawlewicz, M., Howell, D.G., 1997. An
417 integrated model for the tectonic development of the frontal Brooks Range and Colville Basin 250
418 km west of the Trans-Alaska Crustal Transect. *Journal of Geophysical Research* 102, 20685–20708.
- 419 Collett, T., Bird, K., Magoon, L., 1993. Subsurface temperatures and geothermal gradients on the
420 North Slope of Alaska. *Cold Regions Science and Technology* 21, 275–293.
- 421 Duller, G., 1997. Behavioural studies of stimulated luminescence from feldspars. *Radiation Mea-
422 surements* 27, 663–694.

- 423 Duller, G.A.T., 1994. A new method for the analysis of infrared stimulated luminescence data from
424 potassium feldspars. *Radiation Measurements* 23, 281–285.
- 425 Durrani, S., Prachyabrued, W., Christodoulides, C., Fremlin, J., 1972. Thermoluminescence of
426 Apollo 12 samples: Implications for lunar temperature and radiation histories. *Proceedings of*
427 *the Third Lunar Science Conference* 3, 2955–2970.
- 428 Durrani, S., Prachyabrued, W., Hwang, F., Edgington, J., Blair, I., 1973. Thermoluminescence of
429 Apollo 14 and 16 fines and rock samples. *Thermoluminescence of some Apollo 14 and 16 fines*
430 *and rock samples* 3, 2465–2479.
- 431 Durrani, S.A., Khazal, K.A.R., Ali, A., 1977. Temperature and duration of the shadow of a recently-
432 arrived lunar boulder. *Nature* 266, 411–415.
- 433 Fall, A., Eichhubl, P., Bodnar, R.J., Laubach, S.E., Davis, J.S., 2015. Natural hydraulic fracturing
434 of tight-gas sandstone reservoirs, Piceance Basin, Colorado. *GSA Bulletin* 127, 61–75.
- 435 Fall, A., Eichhubl, P., Cumella, S.P., Bodnar, R.J., Laubach, S.E., Becker, S.P., 2012. Testing
436 the basin-centered gas accumulation model using fluid inclusion observations: Southern Piceance
437 Basin, Colorado. *AAPG Bulletin* 96, 2297–2318.
- 438 Fan, M., Quade, J., Dettman, D., DeCelles, P., 2011. Widespread basement erosion during the
439 late Paleocene-early Eocene in the Laramide Rocky Mountains inferred from $^{87}\text{Sr}/^{86}\text{Sr}$ ratios of
440 freshwater bivalve fossils. *GSA Bulletin* 123, 2069–2082.
- 441 Finn, T.M., 2005. Petroleum systems and geologic assessment of oil and gas in the Southwestern
442 Wyoming Province, Wyoming, Colorado, and Utah. U.S. Geological Survey. chapter Geothermal
443 gradient map of the Southwestern Wyoming Province, southwestern Wyoming, northwestern
444 Colorado, and northeastern Utah.
- 445 Fleming, S., Moss, H., Joseph, A., 1970. Thermoluminescence authenticity testing of some ‘six
446 dynasty’ figurines. *Archaeometry* 12, 57–63.
- 447 Gong, G.L., Li, S.H., Sun, W.D., Guo, F., Xia, B., Lu, B.F., 2010. Quartz thermoluminescence -
448 another potential paleo-thermometer for studies of sedimentary basin thermal history. *Chinese*
449 *Journal of Geophysics* 53, 103–112.

- 450 Grün, R., Tani, A., Gurbanov, A., Koschug, D., Williams, I., Braun, J., 1999. A new method for the
451 estimation of cooling and denudation rates using paramagnetic centers in quartz: A case study
452 on the Eldzhurtinskiy Granite, Caucasus. *Journal of Geophysical Research* 104, 17531–17549.
- 453 Guralnik, B., Ankjaergaard, C., Jain, M., Murray, A., Muller, A., Walle, M., Lowick, S., Preusser,
454 F., Rhodes, E., Wu, T.S., Mathew, G., Herman, F., 2015a. OSL-thermochronometry using
455 bedrock quartz: A note of caution. *Quaternary Geochronology* 25, 37 – 48.
- 456 Guralnik, B., Jain, M., Herman, F., Ankjaergaard, C., Murray, A.S., Valla, P.G., Preusser, F.,
457 King, G.E., Chen, R., Lowick, S.E., Kook, M., Rhodes, E.J., 2015b. OSL-thermochronometry of
458 feldspar from the KTB borehole, Germany. *Earth and Planetary Science Letters* 423, 232 – 243.
- 459 Guralnik, B., Jain, M., Herman, F., Paris, R.B., Harrison, T.M., Murray, A.S., Valla, P.G., Rhodes,
460 E.J., 2013. Effective closure temperature in leaky and/or saturating thermochronometers. *Earth
461 and Planetary Science Letters* 384, 209–218.
- 462 Herman, F., Rhodes, E.J., Braun, J., Heiniger, L., 2010. Uniform erosion rates and relief am-
463 plitude during glacial cycles in the Southern Alps of New Zealand, as revealed from OSL-
464 thermochronology. *Earth and Planetary Science Letters* 297, 183–189.
- 465 Hoyt, H., Miyajima, M., Walker, R., Zimmerman, D., Zimmerman, J., 1971. Radiation dose rates
466 and thermal gradients in the lunar regolith: Thermoluminescence and DTA of Apollo 12 samples.
467 *Proceedings of the Second Lunar Science Conference* 3, 2245–2263.
- 468 Hoyt, H.P., Kardos, J.L., Miyajima, M., Seitz, M.G., Sun, S.S., Walker, R.M., Wittels, M.C., 1970.
469 Thermoluminescence, X-ray and stored energy measurements of Apollo 11 samples. *Proceedings
470 of the Apollo 11 Lunar Science Conference* 3, 2269–2287.
- 471 Huntley, D., Baril, M., 1997. The K content of the K-feldspars being measured in optical dating or
472 in thermoluminescence dating. *Ancient TL* 15, 11–13.
- 473 Huntley, D.J., 2006. An explanation of the power-law decay of luminescence. *Journal of Physics:
474 Condensed Matter* 18, 1359–1365.
- 475 Huntley, D.J., Lamothe, M., 2001. Ubiquity of anomalous fading in K-feldspars and the measure-
476 ment and correction for it in optical dating. *Canadian Journal of Earth Sciences* 38, 1093–1106.
- 477 Irwin, D., 1977. Subsurface cross-sections of Colorado. *Rocky Mountain Association of Geologists*.

478 Jagniecki, E.A., Jenkins, D.M., Lowenstein, T.K., Carroll, A.R., 2013. Experimental study of shortite
479 ($\text{Na}_2\text{Ca}_2(\text{CO}_3)_3$) formation and application to the burial history of the Wilkins Peak Member,
480 Green River Basin, Wyoming, USA. *Geochimica et Cosmochimica Acta* 115, 31–45.

481 Jain, M., Ankjaergaard, C., 2011. Towards a non-fading signal in feldspar: Insight into charge
482 transport and tunnelling from time-resolved optically stimulated luminescence. *Radiation Mea-*
483 *surements* 46, 292–309.

484 Jain, M., Guralnik, B., Andersen, M.T., 2012. Stimulated luminescence emission from localized
485 recombination in randomly distributed defects. *Journal of Physics: Condensed Matter* 24, 385402.

486 Jain, M., Sohpati, R., Guralnik, B., Murray, A., Kook, M., Lapp, T., Prasad, A., Thomsen, K.,
487 Buylaert, J., 2015. Kinetics of infrared stimulated luminescence from feldspars. *Radiation Mea-*
488 *surements* 81, 242–250.

489 Kars, R., Wallinga, J., Cohen, K., 2008. A new approach towards anomalous fading correction for
490 feldspar IRSL dating—tests on samples in field saturation. *Radiation Measurements* 43, 786–790.

491 King, G., Guralnik, B., Valla, P.G., Herman, F., 2016a. Trapped-charge thermochronometry and
492 thermometry: A status review. *Chemical Geology* 446, 3–17.

493 King, G., Herman, F., Lambert, R., Valla, P., Guralnik, B., 2016b. Multi-OSL-thermochronometry
494 of feldspar. *Quaternary Geochronology* 33, 76–87.

495 King, G.E., Herman, F., Guralnik, B., 2016c. Northward migration of the eastern himalayan
496 syntaxis revealed by OSL thermochronometry. *Science* 353, 800–504.

497 Kitis, G., Pagonis, V., 2013. Analytical solutions for stimulated luminescence emission from tun-
498 neling recombination in random distributions of defects. *Journal of Luminescence* 137, 109–115.

499 Li, B., Li, S.H., 2012. Determining the cooling age using luminescence-thermochronology. *Tectono-*
500 *physics* 580, 242–248.

501 McKeever, S.W.S., 1985. *Thermoluminescence of solids*. Cambridge University Press, Cambridge.

502 Mejdahl, V., 1983. Feldspar inclusion dating of ceramics and burnt stones, in: *Third Specialist*
503 *Seminar on TL and ESR Dating*.

504 Mejdahl, V., 1985. Thermoluminescence dating based on feldspars. *Nuclear Tracks and Radiation*
505 *Measurments* 10, 133–136.

506 Mull, C., Roeder, D., Tailleur, I., Pessel, G., Grantz, A., May, S., 1987. Geologic sections and maps
507 across Brooks Range and Artic Slope to Beaufort Sea, Alaska. Geological Society of America.

508 Murray, A., Buylaert, J., Thomsen, K., Jain, M., 2009. The effect of preheating on the IRSL signal
509 from feldspar. *Radiation Measurements* 44, 554–559.

510 Nambu, M., Mikami, K., Tsuchiya, N., Nakatsuka, K., 1996. Thermoluminescence of quartz in
511 the borehole cores from the Minase Geothermal area, Akita Prefecture, Japan. *Journal of the*
512 *Geothermal Research Society of Japan* 18, 39–49.

513 Pagonis, V., Ankjaergaard, C., Jain, M., Chithambo, M.L., 2016. Quantitative analysis of time-
514 resolved infrared stimulated luminescence in feldspars. *Physica B* 497, 78–85.

515 Plachy, A., Sutton, S., 1982. Determination of the dose-rate to quartz in granite, in: PACT, AATA.
516 pp. 188–194.

517 Prokein, J., Wagner, G., 1994. Analysis of thermoluminescent glow peaks in quartz derived from
518 the KTB-drill hole. *Radiation Measurements* 23, 85–94.

519 Rhodes, E., 2015. Dating sediments using potassium feldspar single-grain IRSL: initial methodolog-
520 ical considerations. *Quaternary International* 362, 14–22.

521 Roehler, H.W., 1992. Correlation, composition, areal distribution, and thickness of Eocene strati-
522 graphic units, Greater Green River Basin, Wyoming, Utah, and Colorado. *Geology of the*
523 *Eocene Wasatch, Green River, and Bridger (Washakie) Formations, Greater Green River Basin,*
524 *Wyoming, Utah, and Colorado, U.S. Geological Survey.*

525 Sarkar, S.D., Mathew, G., Pande, K., Chauhan, N., Singhvi, A., 2013. Rapid denudation of higher
526 Himalaya during Late Pliocene, evidence from OSL thermochronology. *Geochronometria* 40,
527 304–310.

528 Schmidt, C., Friedrich, J., Zöller, L., 2015. Thermochronometry using red TL of quartz? Numerical
529 simulation and observations from in-situ drill-hole samples. *Radiation Measurements* 81, 98–103.

530 Sfampa, I., Polymeris, G., Pagonis, V., Theodosoglou, E., Tsirliganis, N., Kitis, G., 2015. Correla-
531 tion of basic TL, OSL and IRSL properties of ten K-feldspar samples of various origins. *Nuclear*
532 *Instruments and Methods in Physics Research B* 359, 89–98.

- 533 Smith, M., Carroll, A., Singer, B., 2008. Synoptic reconstruction of a major ancient lake system:
534 Eocene Green River Formation, western United States. *GSA Bulletin* 120, 54–84.
- 535 Spencer, J.Q., Sanderson, D.C.W., 1994. Mapping thermal exposure by luminescence thermometry.
536 *Radiation Measurements* 23, 465–468.
- 537 Spencer, J.Q.G., Sanderson, D.C.W., 2012. Decline in firing technology or poorer fuel resources?
538 high-temperature thermoluminescence (httl) archaeothermometry of neolithic ceramics from pool,
539 sanday, orkney. *Journal of Archaeological Science* 39, 3542–3552.
- 540 Strickertsson, K., 1985. The thermoluminescence of potassium feldspars—glow curve characteristics
541 and initial rise measurements. *Nuclear Tracks and Radiation Measurements* 10, 613–617.
- 542 Tang, S.L., Li, S.H., 2015. Low temperature thermochronology using thermoluminescence signals
543 from quartz. *Radiation Measurements* 81, 92–97.
- 544 Tsuchiya, M., Atsusue, T., Sakaki, H., 1987. Tunneling escape rate of electrons from quantum well
545 in double-barrier heterostructures. *Physical Review Letters* 59, 2356–2359.
- 546 Tsuchiya, N., Fujino, K., 2000. Evaluation of cooling history of the Quaternary Takidani pluton
547 using thermoluminescence technique, in: *Proceedings of the World Geothermal Congress*, pp.
548 3939–3944.
- 549 Tsuchiya, N., Suzuki, T., Nakatsuka, K., 2000. Thermoluminescence as a new research tool for the
550 evaluation of geothermal activity of the Kakkonda geothermal system, northeast Japan. *Geother-*
551 *mics* 29, 27–50.
- 552 Valla, P.G., Lowick, S.E., Herman, F., Champagnac, J.D., Steer, P., Guralnik, B., 2016. Exploring
553 IRSL₅₀ fading variability in bedrock feldspars and implications for OSL thermochronometry.
554 *Quaternary Geochronology* 36, 55–66.
- 555 Valladas, H., Valladas, G., 1987. Thermoluminescence dating of burnt flint and quartz: Comparative
556 results. *Archaeometry* 29, 214–220.
- 557 Visocekas, R., Spooner, N., Zink, A., Blanc, P., 1994. Tunnel afterglow, fading and infrared emission
558 in thermoluminescence of feldspars. *Radiation Measurements* 23, 377–385.
- 559 Wintle, A., Huntley, D., 1982. Thermoluminescence dating of sediments. *Quaternary Science*
560 *Reviews* 1, 31–53.

- 561 Wintle, A., Murray, A., 2006. A review of quartz optically stimulated luminescence characteristics
562 and their relevance in single-aliquot regeneration dating protocols. *Radiation Measurements* 41,
563 369–391.
- 564 Ypma, P., Hochman, M., 1991. Thermoluminescence geothermometry - a case study of the Otway
565 Basin. *The Australian Petroleum Exploration Association Journal* 35, 312–324.
- 566 Zhang, E., Hill, R.J., Katz, B.J., Tang, Y., 2008. Modeling of gas generation from the Cameo coal
567 zone in the Piceance Basin, Colorado. *AAPG Bulletin* 92, 1077–1106.

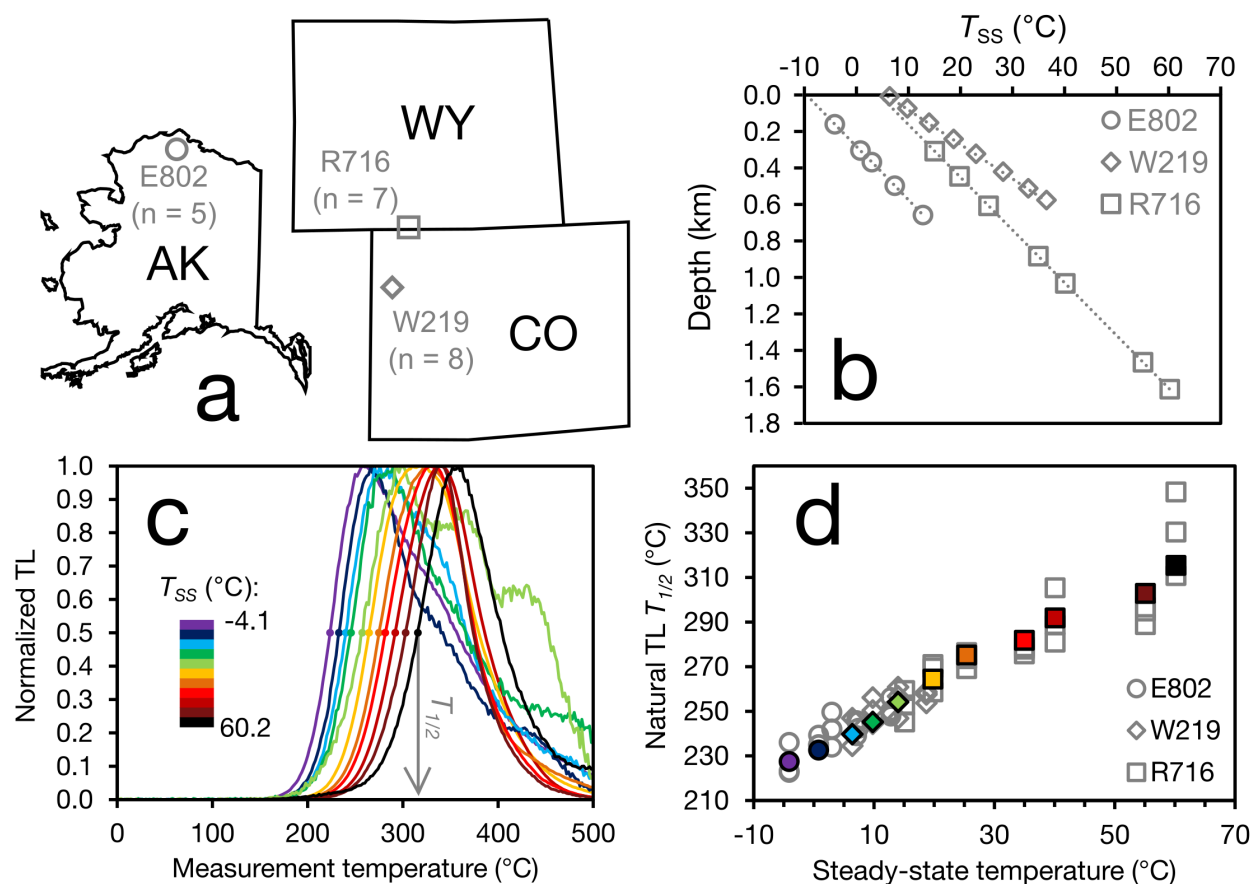


Figure 1: (a) Bedrock sample locations are shown for each of the three USGS CRC drill core sites: E802, W219, and R716. (b) Also shown are the steady-state temperatures for the drill core samples, according to their depths. (c) Representative natural TL signals are colored according to their steady-state temperature, T_{SS} . The $T_{1/2}$ values for these TL curves (normalized to maximum intensity) are shown as solid circles in (c) and are plotted as a function of T_{SS} in (d). The colored symbols in (d) derive from the TL curves shown in (c). The grey symbols represent all of the measured $T_{1/2}$ values, i.e., every aliquots for every sample (see also Fig. 2).

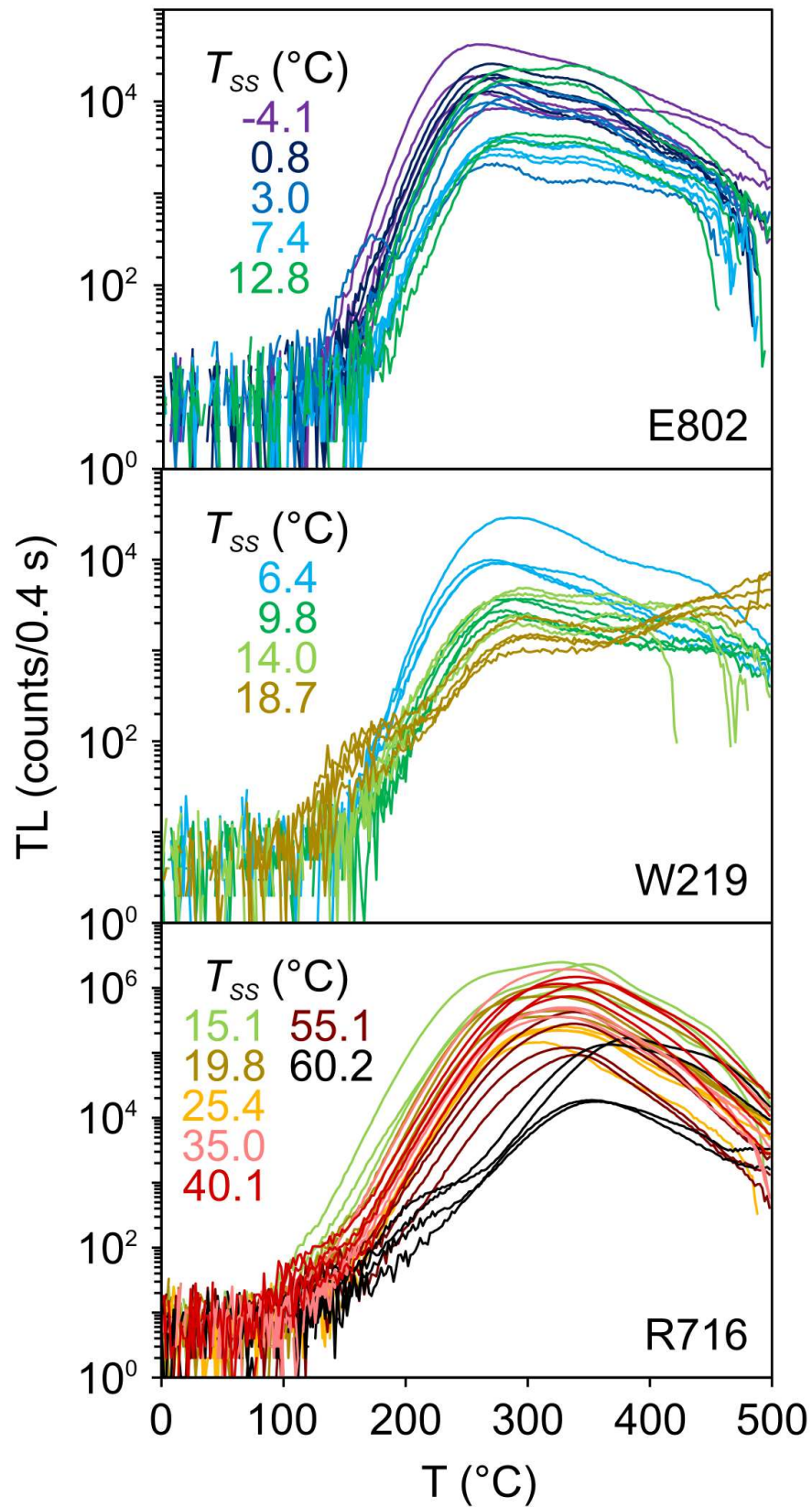


Figure 2: The natural TL signals are plotted by drill core and colored according to the steady-state temperature, T_{SS} (four aliquots are shown per sample). Missing data points within a TL curve signify that the thermal background curve (TL measured after the natural signal and with no dose) at that time bin is larger than the natural signal. Notice the shift in the leading edge and the decreasing brightness as the natural T_{SS} value increases. Notice also the logarithmic y-axes which allow for comparison between the brighter, colder samples and the dimmer samples at higher burial temperatures.

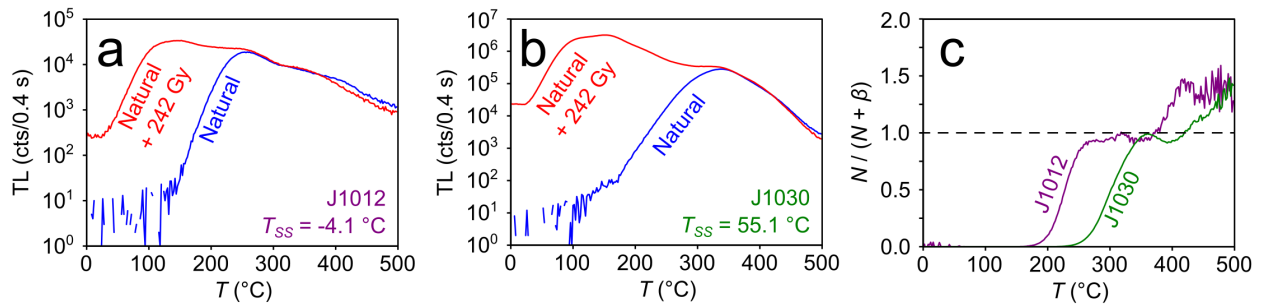


Figure 3: (a) The glow curve shown in blue is a natural aliquot of sample J1012 ($T_{SS} = -4.1^\circ\text{C}$; core E802) ($\beta = 5^\circ\text{C/s}$; the thermal background has been subtracted, so some data points are missing). In red is the TL curve of another aliquot of J1012 that has been given a dose of 242.2 Gy in addition to the natural dose. Notice that the low-temperature portion of the TL glow curve grows with dose, whereas no growth occurs above about 250°C . The same measurements are shown for (b) two aliquots of J1030 ($T_{SS} = 55.1^\circ\text{C}$; core R716). (c) The ratios of the natural response to the added-dose response are plotted as a function of measurement temperature for both samples. A ratio of 1 (dashed line) indicates that the sample is in complete field saturation. Notice how the colder sample is nearly saturated (ratio ~ 0.95) at lower measurement temperatures and saturation occurs at higher measurement temperatures for the sample with a higher burial temperature. Above about 375°C , we see a slight rise in the ratio, which may be attributed to the behavior of a separate, high-temperature peak (Duller, 1997; Murray et al., 2009).

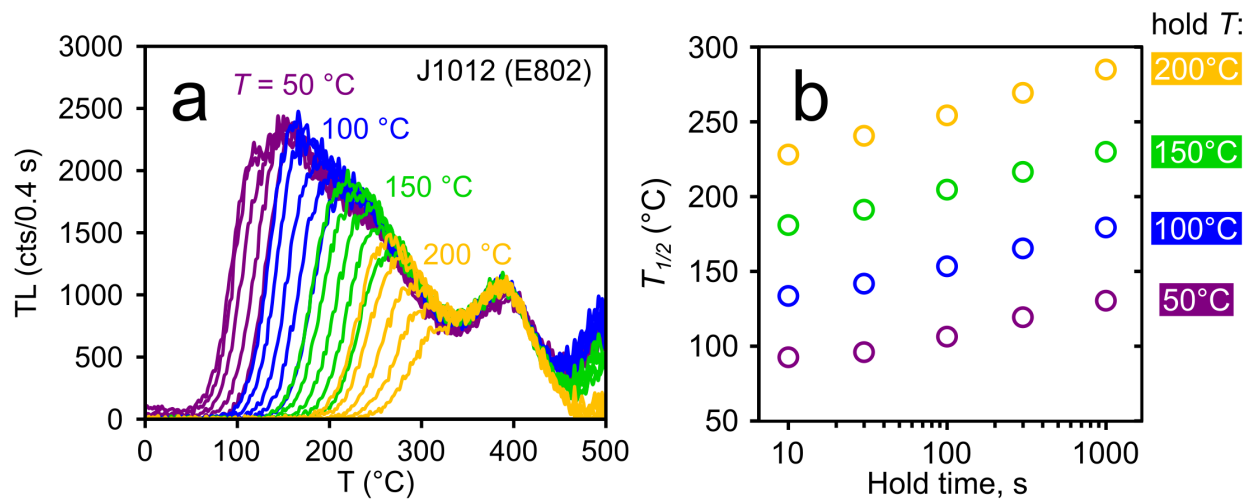


Figure 4: (a) Measured TL curves are shown for sample J1012 (core E802), following isothermal treatments of durations 10, 30, 100, 300, and 1000 s at holding temperatures of 50 (purple curves), 100 (blue), 150 (green), and 200 °C (orange). (b) The $T_{1/2}$ values of these measurements are plotted as a function of hold time and colored according to hold temperature. Notice the shift towards higher $T_{1/2}$ values with longer hold times and higher temperatures.

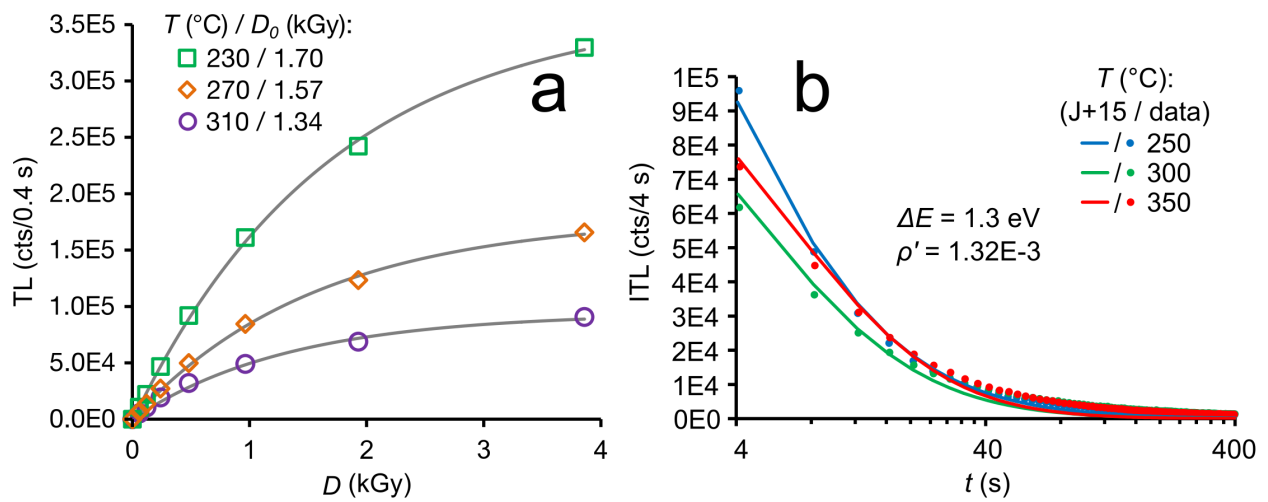


Figure 5: (a) Single-aliquot regenerative (SAR) dose-response measurements of sample J1012 are fitted to a single saturating exponential function. The three TL channels plotted here (230, 270, and 310 °C) represent the observed range of natural $T_{1/2}$ values. The fitted D_0 values at increasing measurement temperatures decrease from 1.70 to 1.34 kGy. (b) The isothermal thermoluminescence (ITL) decay data from sample J1012 following a beta dose of 121 Gy are plotted for a hold time of 400 s at hold temperatures of $T = 250, 300,$ and 350°C . These decays are fitted to the expression for isothermal decay (Eq. 6) from Jain et al. (2015) ('J+15'), using the parameters listed in Table 2 and varying only the initial population (n_0) and the initial lifetime (τ_0) values from one temperature to the next.

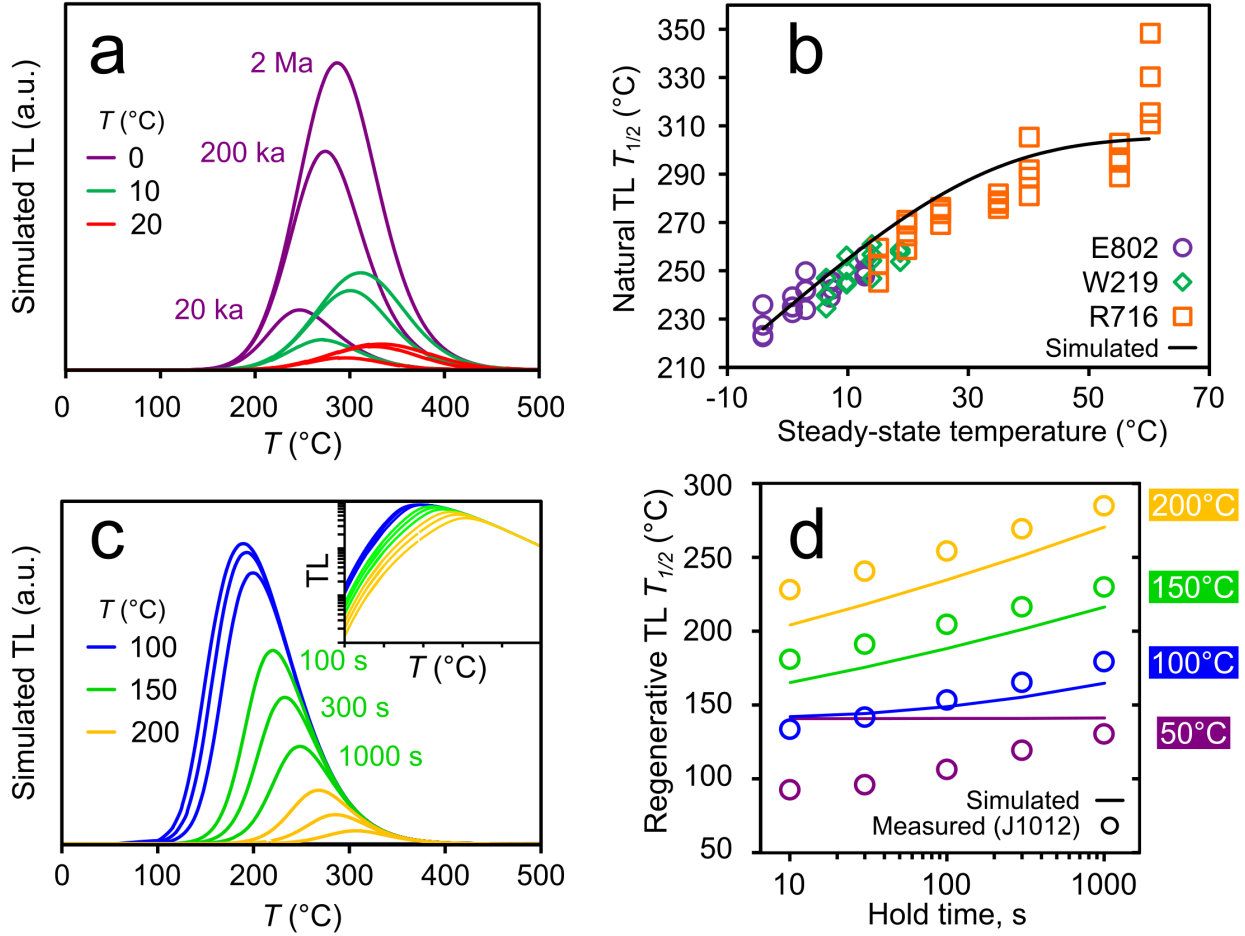


Figure 6: (a) Starting with empty traps, Eq. 1 is solved for isothermal geologic histories. The trapped populations at the final times then become the initial condition for another evaluation of Eq. 1 representing the TL measurement. These are the plotted curves. (Note that after 2 Ma, $n/N \sim 1$ for the most stable traps). (b) This simulation is repeated for each of the steady-state temperature values and the resulting TL $T_{1/2}$ values (solid curve) are compared to the measured $T_{1/2}$ values (open symbols). (c) Instead of reproducing a geologic dose, this experiment reproduces a laboratory dose followed by an isothermal treatment. The simulated TL measurements are shown according to the isothermal conditions. The inset shows a logarithmic y-axis for comparison with Fig. 2. (d) The simulation results from panel (c) are compared against the measured values from sample J1012 (also shown in Fig. 4). For the simulation of geologic and laboratory conditions, the parameters from Table 2 are used.

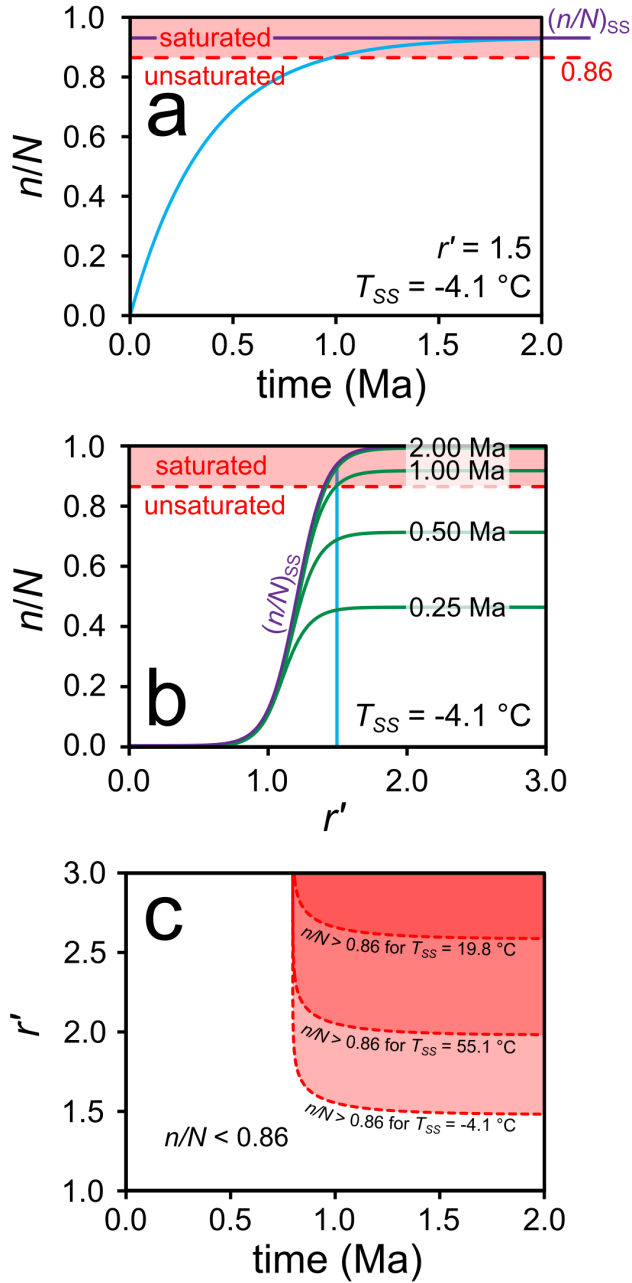


Figure 7: (a) For an arbitrary recombination distance of $r' = 1.5$, trap filling is simulated for 2 Ma at -4.1 °C (T_{SS} for J1012) by assuming an initially empty $n(r')$ distribution that evolves with time according to Eq. 1. After about 1 Ma, the sites at this distance are effectively saturated. Notice that in steady-state at this temperature, not all of the traps will be full, even though they are in steady-state. We illustrate this steady-state limit ($(n/N)_{SS}$) with a purple line. This represents the upper-limit for the concentration of trapped electrons at this temperature. (b) This process is then shown for a range of recombination distances within a lattice, at the same constant temperature ($T = -4.1$ °C). The sites with the greatest recombination distances reach effective saturation ($n/N > 0.86$) first, while those with nearer recombination centers remain unsaturated ($n/N < 0.86$). Importantly, though all distances have reached their steady-state concentration after about 2 Ma, and will not fill any further unless the temperature lowers. (The single distance illustrated in (a) is shown in light blue.) (c) The saturation domain ($n/N > 0.86$) is modeled for three burial temperatures experienced by the drill core samples (the same samples for which MAAD saturation measurements are shown in Fig. 3). Notice that with higher burial temperatures only the trapping sites with high r' values are occupied.